Astron. Astrophys. 227, 634–639 (1990)

ASTRONOMY
AND
ASTROPHYSICS

Imaging using HURA coded apertures with discrete pixel detector arrays

K. Byard, A.J. Dean, A. Goldwurm, C.J. Hall, J.S.J. Harding, and F. Lei

Department of Physics, The University of Southampton, Southampton SO9 5NH, U.K.

Received August 1, 1988; accepted May 18, 1989

Abstract. Hexagonal uniformly redundant array (HURA) coded apertures have important properties for γ-ray imaging and they have been successfully used in conjunction with an Anger camera for astronomical γ-ray observations. However, when coupled to a detector plane constructed from discrete pixels, an inherent systematic noise due to the non-perfect overlap between mask elements and detector pixels can cause degradation of the image quality. Here we present the results of computer simulations designed to evaluate the basic performance of a system employing a rotating HURA mask and two discrete pixel detector geometries; a square pixel detector (SPD) and a hexagonal pixel detector (HPD). Intrinsic systematic noise has been found to affect the quality of the system point spread function for both detector geometries. The noise varies with the mask orientation, the detector resolution and the source position, and is highly magnified by the background level. Special configurations for the HPD geometry have been identified for which a nearly perfect overlap of mask elements with detector pixels occurs at two mask orientations. Under these conditions the systematic noise is completely absent.

Key words: γ-rays – coded masks – image processing

1. Introduction

Coded aperture imaging is now a well known modulation technique to obtain high quality astronomical images in the energy range of hard X-rays and γ-rays where focussing is not feasible. A mask of transparent and opaque elements modulates the radiation incident on a position sensitive detector. Correlation of the recorded data with the mask pattern enables an image of the sky to be reconstructed by suitable deconvolution algorithms. The theory of coded aperture imaging is well advanced and several experiments have demonstrated its capabilities [for a recent review on the subject and classical references see Caroli et al. (1987)].

One of the most recent attempts to optimise the characteristics of coded aperture telescopes consists of employing masks based on hexagonal uniformly redundant arrays (HURA) (Finger and Prince, 1985; Cook et al., 1984). These masks, besides being built on skew Hadamard sets and thus having a system point spread function (SPSF) with flat side lobes, possess other interesting properties. They are antisymmetric upon a 60° rotation and therefore an antimask image can be easily obtained and used to remove systematic effects due to non uniform background (McConnell et al., 1982). Continuous mask rotation also blurs out the ambiguous source repetitions, caused by an excessive repetition of the mask basic pattern, into a low ring centred on the real source peak. Therefore a large field of view (FOV) can be obtained by enlarging the mask without increasing the detection area or reducing the angular resolution. Moreover, the hexagonal geometry makes HURAs particularly suitable for detectors of circular shape. A HURA mask has been successfully used with an Anger camera in a balloon borne imaging telescope for γ-rays (GRIP) by the Californian Institute of Technology group (Althouse et al., 1985, 1987; Cook et al., 1985) and a HURA mask has now been proposed for the major γ-ray astronomy ESA project GRASP (Gamma Ray Astronomy wth Spectroscopy and Positioning) (Assessment Study Report of the GRASP project, December, 1986).

However the use of a hexagonal element mask with a discrete pixel detector introduces an intrinsic systematic noise which leads to a degradation in the deconvolved image quality. This noise is derived from the fact that the hexagonal elements of a HURA mask cannot be binned exactly by the detector pixels, unlike stationary square mask elements with square detector pixels, where binning is perfect. The implication of this mismatch is that the detector will record an asymmetric blurring of the mask shadow, and the correlation between the detector pixels and the mask elements will not be perfect in the deconvolution process.

We have studied the basic performance of a coded system employing a stationary and a rotating HURA mask and a discrete pixel detector plane. Two detector geometries have been studied and compared; a square pixel detector array (SPD) and a hexagonal pixel detector array (HPD). The hexagonal geometry has been studied with the aim of finding a configuration for which the overlap of mask elements and pixels is optimum. In fact a special configuration exists for which at two mask orientations the overlap of hexagonal mask elements with hexagonal pixels is nearly perfect. For this configuration the systematic noise has been found to be completely absent. Here we present the results of computer simulations carried out to study the image quality and in particular the variations of the systematic noise under different observational conditions and different signal to noise ratio levels for the two detector geometries. Section 2 illustrates the characteristics of the imaging system, the deconvolution method used and the way the image quality is evaluated. In Sect. 3 we present the results of the simulations of the SPSF in different observational

Send offprint requests to: A. Goldwurm, Institut de Recherche Fondamentale, Département de Physique Générale, Commissariat à l'Energie Atomique, DPhG/SAp, CEN-Saclay, F-91191 Gif-sur-Yvette Cedex, France

conditions and of a pointlike source in different conditions of background level. In Sect. 4 a brief summary of the conclusions is given.

Experimental tests with a HURA mask and a discrete pixel detector have also been carried out and the results confirm the conclusions reached by the simulations. These experimental results and other computer and laboratory tests done to study different techniques for the reduction of the systematic effects for this kind of coded systems (weighted deconvolution, use of mask and antimask, etc.) will be presented elsewhere (Goldwurm et al., 1990).

2. Imaging requirements

Monte Carlo simulation programs have been developed and used to study the basic imaging performance of an ideal coded aperture system consisting of a HURA mask and a perfect discrete pixel detector plane. The mask used is of 19 element basic pattern and 217 elements in total (Cook et al., 1984), and has been used in conjunction with a square pixel detector array (SPD) and a hexagonal pixel detector array (HPD). The detectors are circular with the useful region having the same size and orientation as the basic mask pattern. The detector efficiency and the closed mask element opacity have both been assumed to be 100%.

Mask rotation has been simulated in steps with the orientation angle α being the angle of orientation of the mask with respect to the detector plane. In the SPD case, α is the angle of the e_0-axis of the hexagonal mask grid with respect to the x-axis of the SPD grid, as shown in Fig. 1 a, so that when $\alpha = 0°$, these axes are coincident. In the HPD case, special detector configurations have been chosen such that two mask orientation angles give a near perfect binning of the mask elements by the detector pixels (Fig. 1 b). One of these angles is chosen as $\alpha = 0°$ and all other mask orientations are measured from this starting point. Because of the difference in geometry of the two detectors, there is no relationship between the value of α of one detector to that of the other. One rotated mask image consists of the sum of six separate stationary mask images at 10° to each other.

The detector resolution is defined by the relative area of mask elements to detector pixels (A_r). The simulations have been carried out having the mask element size (flat to flat) equal to N times the pixel size for the SPD (where N is an integer number) and equal to $\sqrt{[3(N+1)/2][3(N+1)/2-1]}-1$ times the pixel size (flat to flat) for the HPD (where N, in this case, must be an odd integer). In all the simulations, except those for different A_r, N was chosen equal to 5, giving slightly different relative areas in the two cases ($A_r = 21.7$ for SPD, and $A_r = 19$ for HPD).

Deconvolution has been performed by using the finely sampled balanced correlation technique (Fenimore and Weston, 1981; Fenimore and Cannon, 1981), where each pixel flux is projected back to each source bin and either added or subtracted depending on whether the mask cell is open or closed. Each detector pixel is correlated with the mask element in which its centre is projected back. Because of the non-perfect overlap of the mask elements with detector pixels, this standard deconvolution technique is expected to produce some systematic noise which is inherent in the imaging system, unlike an optimum system where overlap is perfect (Gunson and Polychronopulos, 1976). The deconvolved images exhibit a peak with a broad base corresponding to the source position, and repetitions of this source periodically spaced throughout the image (Finger and Prince, 1985). Therefore the image quality has been calculated using the area of the image lying just outside the base of the source peak and inside a circle stretching out as far as possible without including any part of any of the repetitions.

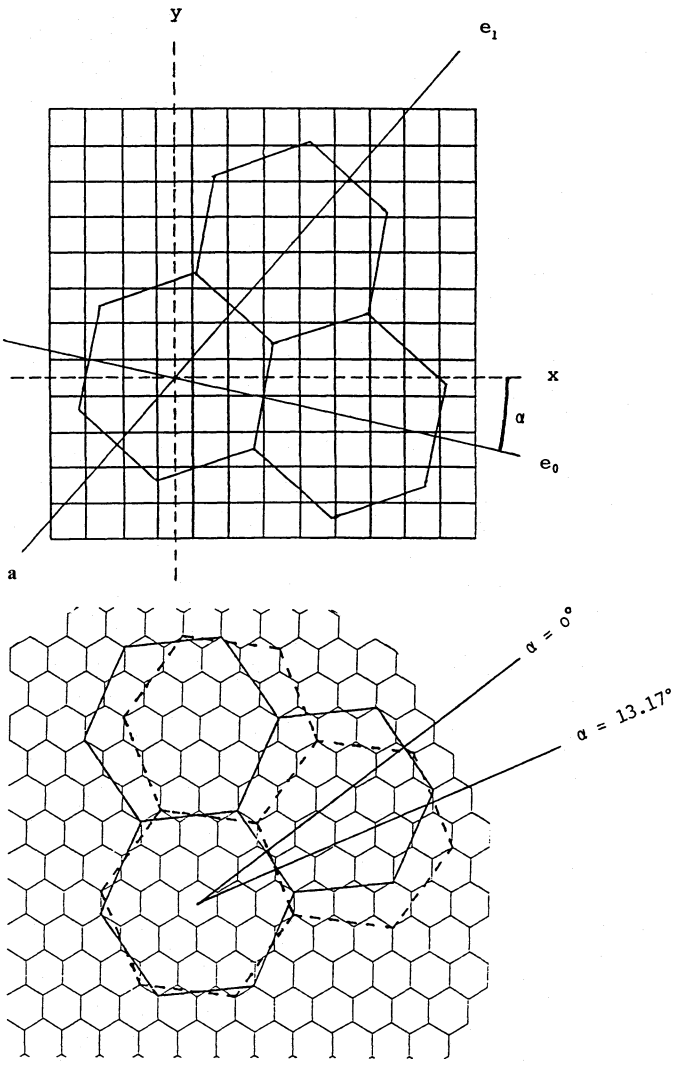

Fig. 1 a and b. Mask element and detector pixel configurations for the SPD (**a**), and the HPD (**b**). For the SPD, the mask rotation angle α is the angle of the e_0-axis of the hexagonal mask grid with respect to the x-axis of the SPD grid. For the HPD, the relative size of the detector pixels to the mask elements has been chosen so that there is a near perfect binning of one by the other as shown in the figure. The mask rotation angle α between the two hexagonal grids is chosen to be 0° when this overlap occurs. Also shown is another angle ($\alpha = 13°17$) for which the near perfect overlap occurs again

The image quality itself has been quantified by calculating the signal to noise ratio, SNR, defined by:

$$\mathrm{SNR} = (P - B)/\sigma_b,$$

where P is the source peak pixel flux value, B is the mean background noise per pixel and σ_b is the standard deviation in the deconvolved background. For a statistical point source in the presence of background the SNR of the deconvolved images obtained by an optimum coded system is expected to vary around the value:

$$\mathrm{SNR}_{exp} = C_s/\sqrt{C_s + C_b},$$

where C_s is the total detector source counts and C_b the total background counts (Carter et al., 1982). When a systematic effect produces a noise comparable or higher than the statistical noise the SNR becomes lower than SNR_{exp}.

3. Computer simulations

The computer simulations have been divided into three sections, namely: (1) system point spread function, (2) statistical source and background, (3) case of nearly perfect overlap for the HPD.

The system point spread function (SPSF) of an imaging system is the response of the system when observing a non-statistical point source in the fully coded field of view in the absence of background noise. Therefore, for a perfect imaging system the SPSF is a pyramidal function and SNR is infinite. For an imperfect system, the systematic noise varies with different observational situations and this noise has been studied and quantified neglecting statistical variations and background noise. For the SPSF the imaging quality has been studied under conditions of varying mask orientation angle, different source position, and varying detector position resolution.

Simulations have also been carried out of observations of a statistical point source in the presence of background noise for both stationary and rotating mask images.

Finally, the case of nearly perfect mask element binning by the HPD has been studied to see the possible reduction in systematic noise using this special geometry.

3.1. Results of simulations: SPSF

The SNR of the SPSF has been calculated for a randomly positioned point source in the fully coded field of view at different mask orientations, α, between 0° and 60° using both detector geometries.

The results are shown in Figs. 2 and 3, where Fig. 2 is the graph of SNR versus α produced by the SPD and Fig. 3 is the corresponding graph for the HPD. In both cases, the SNR varies irregularly and rapidly with no apparent periodicity within the 60° range studied up to 40% from the mid SNR (i.e. the value mid way between the highest and lowest SNR values). The fact that the SNR is not infinite is due to the non-perfect overlap of detector pixels with the mask elements which produces systematic noise. For a fixed source position significant changes in geometrical correlation between pixels and mask elements is expected to occur for changes in mask orientation of $\Delta\alpha >$ (half pixel/mask radius), which is about 1° in our case. In fact high variations in SNR are observed on angular scales of >1° (Fig. 2). In the HPD case, however, the SNR approaches infinity at the two mask orientations angles ($\alpha = 0°$ and $\alpha = 13°2$) for which detector pixels are well matched by mask elements, indicating that systematic noise is effectively absent in these cases.

The SNR has been studied for different source positions around the centre of the field of view, and for larger displacements in a straight line across the whole field of view. Source movements inside an area of approximately one mask element gave only a small SNR range in each case (<7%). Higher variations have been observed for larger displacements. Figure 4 shows the variations in SNR moving the source across the FOV in the case of the HPD for 3 different mask orientations. Changes up to 20% are present, but the mean noise level is clearly determined by the mask orientation rather than by the source position.

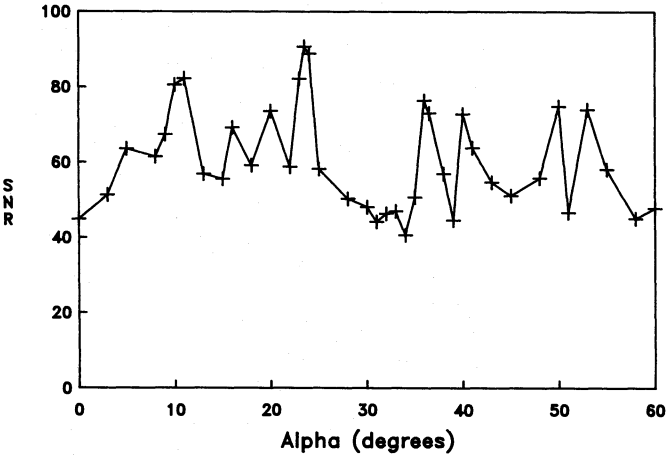

Fig. 2. SNR of the SPSF vs. mask orientation, α, for a non-central point source observed with a stationary mask and the SPD. The mid value SNR is 65.7 and the range is 50.1. Because the SPSF is a non-statistical property of an imaging system, there are no error bars with the datapoints

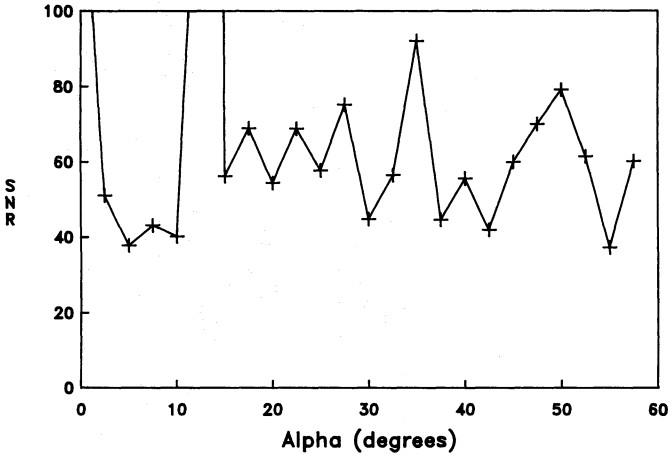

Fig. 3. SNR of the SPSF vs. mask orientation, α, for a non-central point source observed with a stationary mask and the HPD. The mid value SNR (excluding the two large peaks) is 64.6 and the range 54.8. Two large peaks are present at the angles 0° and 13°17 corresponding to the near perfect mask element – detector pixel overlap situation. For these angles the systematic noise is absent

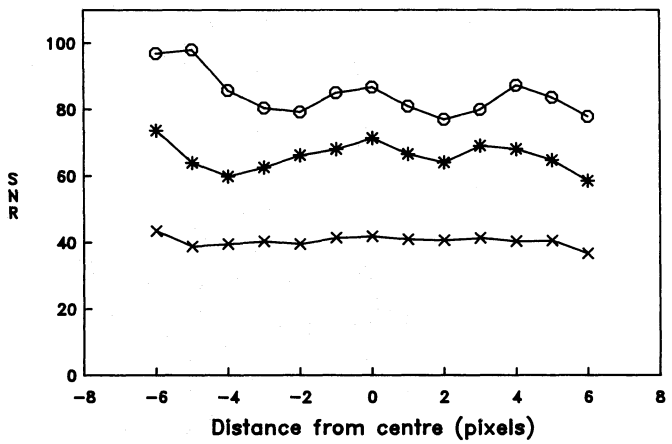

Fig. 4. SNR of the SPSF vs. source position for the HPD. Each curve corresponds to a different mask orientation angle (35° = circles, 45° = asterisks, 55° = crosses). Changes of up to 20% are observed but the mean noise level is clearly determined by the mask orientation

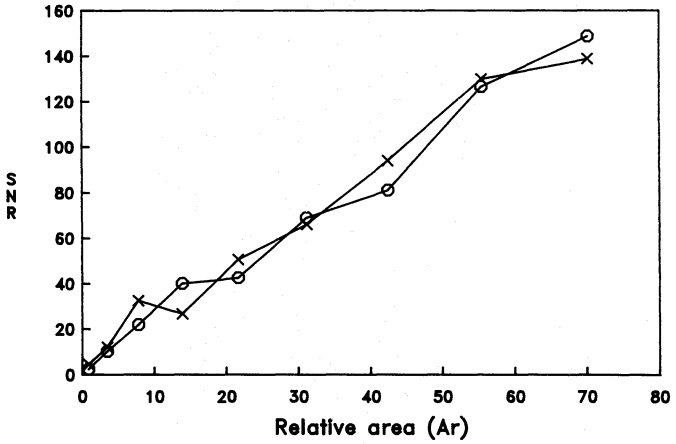

Fig. 5. SNR of the SPSF for the SPD for different detector positional resolutions. The SNR is plotted against the ratio of mask element area to detector pixel area (A_r) for two mask orientation angles, $\alpha = 43°$ (crosses) and $\alpha = 33°$ (circles)

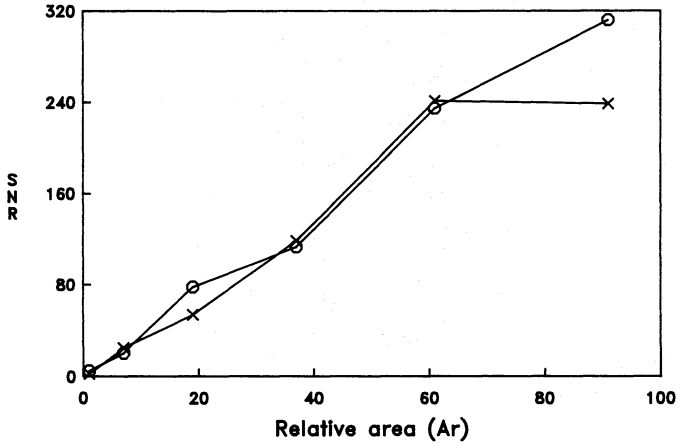

Fig. 6. SNR of the SPSF for the HPD at different detector positional resolutions. The SNR is plotted against the ratio between mask element area and detector pixel area (A_r) for two mask orientation angles, $\alpha = 25°$ (crosses) and $\alpha = 15°$ (circles)

A point source in the centre of the field of view has been studied using different detector position resolutions for both a stationary and a rotated mask for both detectors. The graphs of SNR versus relative area of mask element to detector pixel, A_r, are shown in Figs. 5 and 6 for two mask orientations of each detector. As would be expected, the image quality generally increases with increasing positional resolution due to a better approximation to the "ideal" coded system being achieved at higher resolution. However, at any given mask orientation, geometrical artifacts may occur leading to unexpected trends. Neglecting artifacts, the general trend seems to be approximately linear. This is particularly evident in the graph of Fig. 7, where the SNR vs. A_r is shown for a rotating mask (HPD case), for which the geometrical artifacts occurring at some angles are averaged by the rotation. A regression analysis on the data points shows that each set can be fitted by a straight line with a high correlation coefficient ($=0.98$), giving gradients of 5.0 for the SPD and 6.2 for the HPD. The expected difference in SNR for the two detector geometries (HPD and SPD) due to the slight difference in the detector resolution can therefore be predicted. For rotating mask images with low background level the SNR for the SPD is therefore expected to be about 10% higher than for the HPD.

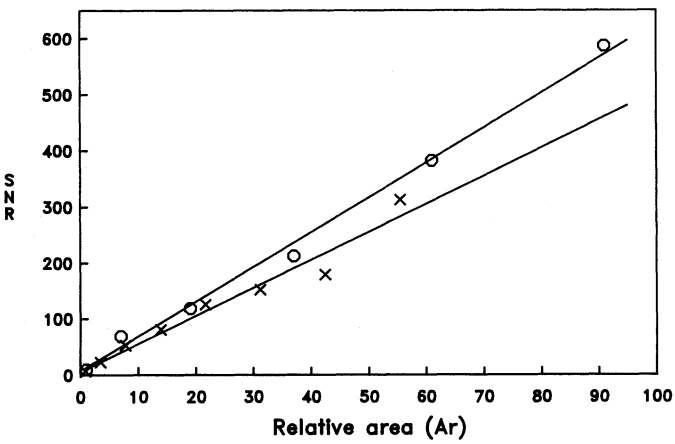

Fig. 7. SNR of the SPSF vs. relative area A_r for a rotating mask. The datapoints and lines of best fit are shown for the HPD (circles) and the SPD (crosses). Their gradients are 6.2 and 5.0 respectively

3.2 Results of simulations: statistical source and background

The same imaging systems have been used to observe a non central point source in the presence of varying levels of background noise for both a stationary and a rotating mask. In all simulations the source flux value was 100 photons per fully illuminated square pixel of the SPD, and a range of background levels up to ten times the source flux was used. The corresponding fluxes used for the HPD were normalised to those of the SPD so that the total detector counts were kept constant for each geometry.

The results of observations using a stationary mask are as follows. Because of the presence of systematic noise, the observed SNR is always less than SNR_{exp} for both detectors, ranging from a 50% decrease at low background up to 90% at higher background. The exceptions to this are at the two angles of near perfect overlap for the HPD (see Sect. 3.3). The SNR decreases with increasing background noise, as would be expected, but the profile versus α has the same general trend as that of the SPSF. This shows that the systematic noise is always overwhelmingly dominant over the statistical noise, even in the case of high background noise. Moreover the background seems to heavily magnify the systematic noise.

For the rotated mask, five trials of observations of a source away from the centre of the field of view have been simulated, and the results are given in Table 1. For each background level studied, the expected SNR, SNR_{exp}, is shown, along with the mean simulated SNR and their corresponding errors. These results are shown graphically (on a logarithmic scale) in Fig. 8. As expected, the SNR decreases with increasing background noise for both detectors, and in all cases is less than SNR_{exp}. This shows that the systematic noise, although decreased by a factor of approximately 2 with respect to that of the stationary mask images, is also present in the rotated mask images, and therefore reduces the image quality. Table 1 also shows the ratio of SNR to SNR_{exp} for each simulation, and it can be seen that this ratio decreases with

Table 1. Rotated mask images

Bkg flux (source flux units)	SNR_{exp}	SPD		HPD	
		SNR	SNR/SNR_{exp}	SNR	SNR/SNR_{exp}
0.0	362	132.3±6.2	0.37	118.6±3.7	0.33
0.1	330	127.7±3.7	0.39	108.2±5.8	0.36
0.5	256	91.8±8.0	0.36	74.6±3.6	0.29
1.0	210	63.8±2.6	0.30	53.9±1.3	0.26
3.0	139	31.7±0.6	0.23	24.8±1.2	0.18
5.0	111	20.0±0.4	0.18	15.5±0.5	0.14
10.0	80	10.2±0.3	0.13	8.1±0.2	0.10

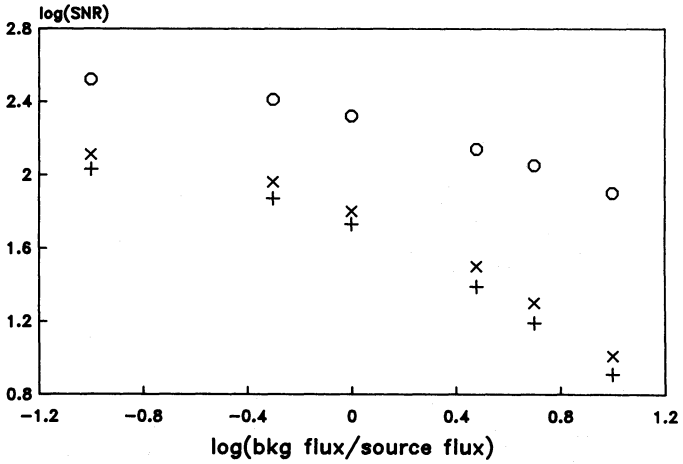

Fig. 8. log(SNR) vs. log(Bkg flux/source flux) for a non-central point source observed using a rotating HURA in conjunction with a SPD (crosses) and a HPD (pluses). The errors in SNR are smaller than the symbols which represent these datapoints, and are therefore not shown. Also shown are the expected SNR values in the absence of systematic noise (circles)

increasing background noise. This implies that the background level magnifies the systematic noise in the deconvolved images.

The SNR is further reduced by an effective loss of source photons. These are photons which originate from the source but are incident on detector pixels which are correlated with opaque mask elements when deconvolving the source sky pixel. The proportion of these "lost" photons is $\simeq 5\%$ for the SPD with $A_r = 21.7$. Thus, by the equation for SNR_{exp} given in Sect. 2, the SNR is expected to fall by 5%, a negligible decrease, however, compared to that produced by the systematic noise.

The SNR values for the SPD are between 10% and 20% higher than those of the HPD. This may be due to the relative area A_r being higher for the SPD giving a finer positional resolution. As already pointed out (Sect. 3.1) such differences in resolution can lead to the changes observed.

3.3 Results of simulations: case of near perfect overlap for the HPD

Five observation trials of the same non central source were simulated for the HPD using the mask orientations of near perfect overlap, $\alpha = 0°$ and $\alpha = 13.^{\circ}17$. The background levels used were the same as those in the previous section. The results for $\alpha = 13.^{\circ}17$ are given in Table 2. The expected SNR for each background level lies inside the estimated errors calculated from the five trials at each level. This indicates that with a HPD and a stationary mask oriented at either of the two angles of near perfect overlap, the systematic noise is barely in evidence. Although there is no systematic noise, there is still an effective loss of source photons because the overlap is not perfect, giving a SNR less than SNR_{exp}. This reduction is very small, less than 5%, and is therefore not apparent from the results given in Table 2 since statistical fluctuations are of the order of 10%. Other simulations of the SPSF of this system have shown that the SNR tends to infinity, and does not change with source position or detector resolution.

Table 2. SNR of stationary mask images at $\alpha = 13.^{\circ}17$ for the hexagonal pixel detector

Bkg flux (source flux units)	SNR_{exp}	SNR
0.0	148	167±19
0.1	135	142±17
0.5	104	112±17
1.0	86	83±11
3.0	57	57± 9
5.0	45	46± 5
10.0	32	34± 4

A rotating mask incorporating these optimum angles was also used to observe the same source as in Sect. 3.2. A clear improvement (>40%) was seen only when using both of the optimum angles to build a rotating mask image. However, when incorporating only one of these angles, inconsistent results were obtained, depending on which other angles were used. Moreover for a continuously rotating mask the effect of these optimum mask angles on the quality of the final image is expected to be very low.

4. Discussion and conclusion

When a point source is observed using a HURA mask and a discrete pixel detector, systematic noise is observed to be present in the deconvolved image. This is due to the non-perfect overlap of pixels with the mask elements. Such a mismatch causes the recorded image of the mask shadow to be asymmetrically

distorted by the finite resolution and discrete nature of the detector. It must be pointed out that this blurring is completely different from that which occurs when a source lies on the border of two sky pixels in the FOV of an optimum coded system (also referred to as a phasing error, see Fenimore and Weston, 1981). In this case the blurring is symmetrical in the sense that it occurs in the same way for any projected mask element, so the only effect is a blurring of the source peak and no systematic noise is generated in the deconvolved images. Moreover, in a simple cross-correlation deconvolution the deconvolution array has the same geometry as the detector array and therefore it is only an approximation to the real hexagonal mask pattern. The sky pixels are reconstructed by correlating the detector array with different parts of this deconvolution array. Because of the discrete subdivision of the mask, some photons which should be correlated with an open mask element instead become correlated with a closed one and vice versa, and an error is introduced in the reconstruction of the source counts for off-source sky positions. Because different sky pixels correspond to different subsets of the deconvolution array, the number of closed cells varies from subset to subset. Thus, different proportions of the background will be subtracted for different sky pixels giving a systematic error for the background also, the magnitude of which depends on the background level, and being dominant for higher background counting rates.

As expected the higher the detector resolution the better the geometrical correlation between pixels and mask elements and therefore the lower the systematic noise. The noise was found to decrease linearly with the number of pixels per mask element, with gradients of SNR vs. A_r of 5.0 for the SPD and 6.2 for the HPD in the case of the rotated mask, both curves passing close to the origin. For both detector geometries the systematic noise also depends on the mask orientation and source position and is highly magnified by the background level. In the case of a detector with about 20 pixels per mask element, the SNR of the SPSF fluctuates irregularly with the mask orientation (up to 50% from the mid SNR) and with the source position (up to 20%). For both a stationary and a rotating mask the reduction of the SNR with respect to the SNR expected for pure statistical noise ranges from 60% at low background levels to 90% for input signal to noise ratios of 0.1. Therefore the sensitivity of a telescope using this coded system can be drastically reduced particularly if it works in the energy range of γ-ray astronomy where the signal to noise ratios are typically of the order of 10^{-2}–10^{-3}.

In the case of a rotating mask, the problem cannot be avoided using a particular detector geometry, and more sophisticated deconvolution techniques must be applied. Although other deconvolution techniques [such as the use of a Wiener filter, or the maximum entropy method, see Willingale et al. (1988)] may give better results, one can improve the correlation by reducing the error due to the decoding array both for the source and for the background counts, as we will show elsewhere (Goldwurm et al., 1990). For a stationary mask, however, we have found that for a detector array of hexagonal pixels with a special ratio of pixel size to mask element size, the mask can be oriented in such a way that the overlap between mask elements and pixels is nearly perfect and hence the systematic noise is completely absent. This configuration has been adopted for the coded aperture system of the GRASP telescope, in which a stationary HURA mask (basic order 79) is associated with a circular composite detector plane consisting in CsI hexagonal bars and circular germanium spectrometers.

Acknowledgements. Andrea Goldwurm acknowledges receipt of the S.E.R.C. Visiting Fellowship GR/E37538 and the Angelo delle Riccia Fellowship which have jointly financed his stay at Southampton. Lei Fan wishes to express his gratitude to the Academia Sinica, Peoples Republic of China, for the provision of funds allowing him to study within the U.K.

References

Althouse, W.E., Cook, W.R., Cummings, A.C., Finger, M.H., Prince, T.A., Schindler, S.M., Starr, C.H., Stone, E.C.: 1985, Proc. 19th Internat. Cosmic Ray Conf., La Jolla, **3**, 299

Althouse, W.E., Cook, W.R., Cummings, A.C., Finger, M.H., Palmer, D.M., Prince, T.A., Schindler, S.M., Starr, C.H., Stone, E.C.: 1987, Proc. 20th Internat. Cosmic Ray Conf., Moscow, OG 2.1-12

Caroli, E., Stephen, J.B., Di Cocco, G., Natalucci, L., Spizzichino, A.: 1987, *Space Sci. Rev.* **45**, 349

Carter, J., Ramsden, D., Frye, G.M., Jenkins, F.L., Koge, R.: 1982, M.N.R.A.S., **198**, 33

Cook, W.R., Finger, M.H., Prince, T.A., Stone, E.C.: 1984, *IEEE Trans. Nucl. Sci.*, NS-**31**, No. 1, 771

Cook, W.R., Finger, M.H., Prince, T.A.: 1985, *IEEE Trans. Nucl. Sci.*, NS-**32**, No. 1, 129

Fenimore, E.E., Cannon, T.M.: 1978, *Appl. Optics* **17**, No. 3, 337

Fenimore, E.E.: 1978, *Appl. Optics* **17**, No. 22, 3562

Fenimore, E.E.: 1980, *Appl. Optics* **19**, No. 14, 2465

Fenimore, E.E., Weston, G.S.: 1981, *Appl. Optics* **20**, No. 17, 3058

Finger, M.H., Prince, T.A.: 1985, Proc. of the 19th Int. Cosmic Ray Conf., La Jolla, OG 9.2-1, 295

Goldwurm, A., Byard, K., Dean, A.J., Hall, C.J., Harding, J.S.J.: 1990, *Astron. Astrophys.* **227**, 640

Gunson, J., Polychronopulos, B.: 1976, M.N.R.A.S. **177**, 485

McConnell, M.L., Forrest, D.J., Chupp, E.L., Dunphy, P.P.: 1982, *IEEE Trans. Nucl. Sci.* NS-**29**, No. 1, 155

Willingale, R., Sims, M.R., Turner, M.J.L.: 1984, *Nucl. Instr. Meth. Phys.* **221**, 60